Changes in tree drought sensitivity provided early warning signals to the California 1 drought and forest mortality event 2

Article *in* Global Change Biology · October 2021

DOI: 10.1111/gcb.15973

Rachel Keen
Kansas State University

Steven L Voelker
Michigan Technological University

Shih-Yu Simon Wang
Utah State University / Utah Climate Center

Barbara Bentz
Rocky Mountain Research Station, US Forest Service

Changes in tree drought sensitivity provided early warning signals to the California drought and forest mortality event

Rachel M. Keen[1*], Steven L. Voelker[2], S.-Y. Simon Wang[3], Barbara J. Bentz[4], Mike Goulden[5], Cody R. Dangerfield[6], Charlotte C. Reed[7], Sharon M. Hood[7], Adam Z. Csank[8], Todd E. Dawson[9], Andrew G. Merschel[10], Christopher J. Still[10]

1. Division of Biology, Kansas State University, Manhattan, KS, USA

2. Department of Environmental and Forest Biology, SUNY ESF, Syracuse, NY, USA

3. Department of Plants, Soils and Climate, Utah State University, Logan, UT, USA

4. USDA Forest Service, Rocky Mountain Research Station, Logan, UT, USA

5. Department of Earth System Science, University of California, Irvine, CA, USA

6. Department of Wildland Resources, Utah State University, Logan, UT, USA

7. USDA Forest Service, Rocky Mountain Research Station, Fire Sciences Laboratory, Missoula, MT, USA

8. Department of Geography, University of Nevada, Reno, NV, USA

9. Department of Environmental Science, Policy & Management, University of California, Berkeley, CA, USA

10. Department of Forest Ecosystems and Society, Oregon State University, Corvallis, OR, USA

*Corresponding author – Email: rlease@ksu.edu

Abstract

Climate warming in recent decades has negatively impacted forest health in the western United States. Here, we report on potential Early Warning Signals (EWS) for drought-related mortality derived from measurements of tree-ring growth and carbon isotope discrimination ($\Delta^{13}C$), primarily focused on ponderosa pine (*Pinus ponderosa*). Sampling was conducted in the southern Sierra Nevada Mountains, near the epicenter of drought severity and mortality associated with the 2012-2015 California drought and concurrent outbreak of western pine beetle (*Dendroctonus brevicomis*). At this site, we found that widespread mortality was presaged by five decades of increasing sensitivity (i.e., increased explained variation) of both tree growth and $\Delta^{13}C$ to Palmer Drought Severity Index (PDSI). We hypothesized that increasing sensitivity of tree growth and $\Delta^{13}C$ to hydroclimate constitute EWS that indicate an increased likelihood of widespread forest mortality caused by drought stress or drought-diminished host defenses. We then tested these EWS in additional ponderosa pine-dominated forests that experienced varying mortality rates associated with the same California drought event. In general, drier sites showed increasing sensitivity of RWI to PDSI over the last century, as well as higher mortality following the California drought event compared to wetter sites. Two sites displayed evidence that thinning or fire events that reduced tree basal area effectively reversed the trend of increasing hydroclimate sensitivity. These comparisons indicate that reducing competition for soil water and/or decreasing bark beetle host-tree density via forest management – particularly in drier regions – may buffer these forests against drought stress and associated mortality risk. EWS such as these could provide land managers more time to mitigate the extent or severity of forest mortality in advance of droughts. Substantial efforts at deploying additional dendrochronological research in concert with remote sensing and forest modeling will aid in forecasting of forest responses to continued climate warming.

Key Words: drought; conifer mortality; Sierra Nevada Mountains; carbon isotope discrimination; ponderosa pine; western pine beetle

1. Introduction

In recent decades, climate warming and increased aridity have negatively impacted forest health and water availability across the western United States and elsewhere around the globe (Allen et al. 2010; Williams et al. 2013; Millar and Stephenson 2015; Williams et al. 2020; Martin et al. 2020). These aridity trends are projected to continue, resulting in more severe and/or frequent droughts and large-scale forest mortality events in the future (Sperry et al. 2019; Xu et al. 2019). Increasing tree mortality rates associated with the combined influence of prolonged drought and bark beetle outbreaks – including massive dieback events like those seen in California over the past decade – can be detrimental to the ability of forests to sustain ecosystem functions and harm economically important timber and non-timber industries (van Mantgem 2009; Adams et al. 2010; Anderegg et al. 2013; Trumbore et al. 2015; Morris et al. 2018; Goulden and Bales 2019). It would therefore be of great benefit to forest managers and landowners to develop early warning signals (EWS) that can predict when forests are becoming critically susceptible to widespread drought-related mortality. Forecasting of forest mortality events via EWS could help allocate resources to landscapes or regions where the promotion of resistance and resilience to climate change is deemed most critical. Toward this end, several EWS have been proposed based on both remote sensing products and tree growth patterns (**Table S1**). Prospective EWS that use remote sensing applications (Brodrick and Asner 2017; Goulden and Bales 2019; Liu et al. 2019) hold great promise because of their fast and large-scale mapping capacities and the ever-increasing timescales over which they are available. On the other hand, remote sensing applications may not be appropriate for all forest types or may provide EWS on time scales too short to implement effective management actions at a scale commensurate with the regional-scale impacts of drought and the attendant landscape-scale risk. Annually resolved measurements from tree-ring records are well-suited to provide insight on long-term shifts in environmental stresses that impact tree function. Tree-ring records can complement remote sensing-derived EWS by providing in-situ data to assist in forecasting susceptibility to forest dieback with sufficient time to undertake meaningful management action. However, reliance on a single tree-ring metric carries increased risk of false positive or negative EWS detections for certain species or regions.

For over a century, tree ring-width patterns have been used to infer historical trends in rainfall or drought, as these climate factors affect manifold phenomena impacting growth (Douglass 1914; Fritts 1976). In addition, stable carbon stable isotope discrimination ($\Delta^{13}C$) in tree-rings records the canopy-integrated ratio of photosynthetic assimilation to stomatal conductance (Farquhar et al. 1989; McCarroll and Loader 2004; Ehleringer and Farquhar 1993), making it a promising EWS candidate. In forests of the western United States, $\Delta^{13}C$ has been used extensively to understand various aspects of past drought stress due to the dominant impact of stomatal closure on this signal (Roden and Ehleringer, 2007; Leavitt et al. 2011; Szejner et al. 2016; Voelker et al. 2019; Keen et al. 2020; Schook et al. 2020). Both ring-width and $\Delta^{13}C$ records offer insight into differing dimensions of drought stress that may be important for recognizing novel EWS. Multiple tree-ring properties – such as stable isotopes and growth rates, as well as emergent tree-ring signals – may provide a combination of independent EWS that are helpful in confirming or disconfirming looming threats to forests and provide diagnostic information about the ecophysiological responses leading to mortality or resilience of the affected trees.

Shifts in climate sensitivity of tree-ring widths can occur for several reasons, including non-linear ecophysiological responses to discrete events that may or may not be associated with climate change (Peltier and Ogle 2020). Here, we further contend that long-term shifts in ring-width or stable isotope sensitivity to hydroclimate constitute emergent properties that can yield detectable EWS up to a decade or more ahead of substantially increased likelihood of a widespread forest mortality event, providing sufficient time to enact preventative management strategies (i.e., stand thinning and/or prescribed fire). Cailleret et al. (2019) is the most prominent example of EWS being determined using tree ring properties; they identified increasing variability in growth rates in the two decades prior to tree death as the most effective EWS for identifying individual tree death vs survival. The novel EWS we introduce are not mutually exclusive of such previously proposed EWS since, ideally, multiple diagnostic tools – including some combination of tree-ring, remote sensing, and modeling products – should be used together for the greatest confidence in spatiotemporal projections of increased likelihood of forest mortality. Because water availability is often the most important limiting factor to tree growth (Fritts, 1976), we also incorporate a hydroclimate variable to estimate relative soil dryness as a proxy for two pertinent drought-related risk factors: (1) increased competition for soil water due to increasing stand density, and (2) consistently rising air temperatures associated with climate warming that modify local hydroclimate variability.

The California drought event from 2012-2015 (hereafter referred to as the "CA drought") presents a unique opportunity with which to retrospectively determine whether detectable EWS occurred leading up to the CA drought event and associated western pine beetle (*Dendroctonus brevicomis* Coleoptera: Curculionidae, Scolytinae) population outbreak, which lead to the death of > 150 million trees between 2014 and 2019 (USDA Forest Service 2019). This recent drought was characterized by historically intense soil moisture deficits across much of California (Griffin and Anchukaitis 2014; Williams et al. 2015). This event was also superimposed upon a century of progressively warmer and drier conditions that have resulted in earlier snowmelt and warmer and longer growing seasons (Gleick 1987; Stewart et al. 2004; Knowles and Cayan 2004; Mote et al. 2005; Kukal and Irmak 2018). In particular, low precipitation and high temperatures during the climatic "wet" winter and spring seasons contributed to water deficits that were intensified by longer summer drought periods experienced by these forests for multiple consecutive years (Luo et al. 2017). This anomalous aridity resulted in severe canopy moisture deficit and multi-year deep soil drying in the Sierra Nevada mountains (Asner et al. 2016; Goulden and Bales 2019). These types of conditions are known to contribute to increased host-tree susceptibility to bark beetle attack (Raffa et al. 2008; Kolb et al. 2016, 2019). When combined with warming temperatures, an expansive western pine beetle population outbreak occurred during this drought period, resulting in extensive ponderosa pine (*Pinus ponderosa* Lawson & C. Lawson) mortality in the central and southern Sierra Nevada mountains (Fettig et al. 2019; Pile et al. 2019; Stephenson et al. 2019; Keen et al. 2020; Reed and Hood 2020).

In this study, we utilized tree-ring growth rates and $\Delta^{13}C$ to assess hydroclimate sensitivity in ponderosa pines in the southern Sierra Nevada leading up to the 2012-2015 CA drought and associated mortality event. We hypothesized that two general EWS were present in the decades prior to the drought event – increasing sensitivity of (1) ring width index (RWI) and (2) $\Delta^{13}C$ to hydroclimate, where sensitivity is defined as increasing R^2 of a tree-ring variable vs. hydroclimate through time (**Table 1**). These EWS were then assessed in additional ponderosa pine-dominated mixed conifer sites across California and Oregon to determine their applicability to other drought-impacted regions in the western United States.

2. Methods

2.1 Study area

Sampling was conducted in the spring of 2017 at Soaproot Saddle (SOS), a Southern Sierra Critical Zone Observatory site northeast of Fresno, CA (**Figure 1**). In this area, ponderosa pine-dominated mixed conifer forests occur between ~900 and 2,000 m elevation. SOS is located at 1,160 m elevation and receives ~800 mm of precipitation each year. Mean minimum temperature in this region is 5.5 °C and mean maximum temperature is 18 °C (Goulden et al. 2012). A large portion of annual precipitation occurs in the winter and spring, followed by a summer drought period. Historically, this ecosystem experienced frequent, low-intensity fires every 10-20 years that kept ponderosa pine-dominated forests "open and park-like" (Parsons and DeBenedetti 1979; North et al. 2005; Van de Water and Safford 2011). Since widespread fire suppression efforts have been in place over the past century, most of the forests in this region have transitioned to dense, mixed-conifer forests with higher concentrations of fire-intolerant and shade-tolerant tree species (Stephens et al. 2015).

2.2 Increment core collection, preparation, and measurement

At SOS, twelve large ponderosa pines (> 60 cm DBH) – six live and six recently dead – were sampled using increment borers. For each tree, three 12-mm diameter increment cores were extracted at approximately equal intervals from around the tree circumference at heights ranging between 1.0 and 1.5 m from ground level. Diameter at breast height (DBH) and evidence of western pine beetle attack were recorded for each ponderosa pine. Each increment core was mounted on a wooden stave and sanded using increasingly higher grit sandpaper (120-400) to prepare cores for visual cross-dating and measurement of annual growth rings. Whole ring widths were measured using MeasureJ2X software (Coortech Consulting) and visual cross-dating was conducted to assign calendar years to the rings in each core (Stokes and Smiley 1968). Visual cross-dating was confirmed using COFECHA, a statistical program that assesses cross-dating quality and accuracy (Holmes 1983). Ring width chronologies from SOS were detrended separately using a negative exponential spline first to remove the biological growth signal, then with a spline length set to 66% of the time-series length to isolate climate trends. All detrending was conducted in ARSTAN (Cook and Krusik 2014).

2.3 Stable Isotope Analysis

For each tree core, latewood (which is derived primarily from carbon assimilated in the summer and early autumn; Kagawa et al. 2006) was separated using a scalpel under a dissecting microscope. The latewood portions from cores from each individual tree were combined by calendar year, then each latewood sample was ground with a Wiley mill (80 mesh size) and sealed in a mesh filter bag (mesh size 25 µm; ANKOM Technology, Macedon, NY). α-cellulose was isolated from each sample (Leavitt and Danzer 1993; Rinne et al. 2005), homogenized in deionized water using an ultrasonic probe, and subsequently freeze-dried (Laumer et al. 2009). Samples were then packed in tin capsules before being analyzed at the Center for Isotope Biogeochemistry (CSIB) at the University of California, Berkeley. The carbon isotope ratio of each sample was obtained using standard high temperature combustion in a vario-Pyrocube elemental analyzer interfaced with an IsoPrime/Elementar IsoPrime gas phase isotope ratio mass spectrometer (IsoPrime Ltd., Manchester, UK). The long-term precision does not exceed ± 0.1 ‰ for the mass spectrometer employed at CSIB.

All $\delta^{13}C$ values were converted to carbon isotope discrimination values ($\Delta^{13}C$) following Farquhar et al. (1982):

$$\Delta^{13}C = \frac{\delta^{13}C_{air} - \delta^{13}C_{plant}}{1 + \delta^{13}C_{plant} / 1000}$$

In this equation, $\delta^{13}C_{air}$ was estimated annually from the values given by McCarroll and Loader (2004) merged with more recent $\delta^{13}C_{air}$ records from Mauna Loa, Hawaii.

2.4 Application of EWS to additional sites

To test the generality of our hypothesized EWS, we obtained ring-width data from five additional ponderosa pine-dominated sites within California (**Figure 1**) and one site in Oregon (KEW; after Voelker et al. 2019). All sites experienced drought conditions over the same period but had varying degrees of mortality associated with the drought event. Data were obtained from the International Tree-Ring Database (ITRDB) for the Truckee Ranger Station (TRS) and Fulda Creek (FUC) sites (after Shamir et al. 2020) and for the Sierra National Forest (SNF) site (after Reed and Hood 2020). Additional unpublished data from the Hirschdale Road (HIR) and the upper Truckee River (TCR) sites were also included

(Csank, *unpublished*). Each site, as well as the larger landscape matrix, was characterized by mixed-conifer forests in which ponderosa pine was one of the dominant species, such that enough host trees would have been present to support a western pine beetle population outbreak (similar to conditions at Soaproot Saddle). At SNF, both live and recently killed trees were sampled, whereas at each additional site increment cores were collected from apparently healthy dominant or co-dominant trees.

2.5 Climate and model output data

Climate data used in RWI and $\Delta^{13}C$-hydroclimate sensitivity analyses were derived from various sources. In this study, we employed Palmer Drought Severity Index (PDSI) as a hydroclimate-related variable that integrates temperature and precipitation, providing an estimate of relative soil dryness. Monthly PDSI data for each site were obtained from the WestWideDroughtTracker website (https://wrcc.dri.edu/wwdt/) – these data represent the nearest 4 x 4 km grid cell to the site location data. Other monthly climate data were obtained through ClimateWNA (http://www.climatewna.com/) or PRISM (http://www.prim.oregonstate.edu/). As in Keen et al. (2020), monthly variables were averaged seasonally for winter (previous December, current January and February), spring (March-May), summer (June-August), and fall (September-November). These seasonally-resolved climate data were pre-whitened to remove autocorrelation and long-term trends, and to highlight interannual variation. Most of our analyses employ PDSI because, after screening several other meteorological and hydroclimate variables, it was most closely related to tree-ring growth and $\Delta^{13}C$ (Keen et al. 2020). North Pacific High (NPH) data were the same as in Black et al. (2018). These constituted Hadley Centre HadSLP2 sea level pressure [http://www.metoffice.gov.uk/hadobs/ hadslp2/] observations across a domain encompassing 25°N–35°N by 125°W–145°W and summarized as means across the months of January to March. NPH variability has increasingly driven atmospheric control of cold-season climate (Yoon et al. 2015) and was recently tied to rising synchrony in tree growth in multiple locations across the western United States.

Landsat Normalized Difference Moisture Index (NDMI) were obtained for the years 1984-2016 after Goulden and Bales (2019) for grid cells overlapping the tree-ring sampling locations. To assess the spatial representativeness of regional drought responses we mapped the difference in NDMI (δNDMI) between the dry seasons of 2012 and 2016 across the Sierra Nevada Mountains, which delineated changes in canopy moisture content associated with severe drought conditions and forest canopy mortality between

2012-2015. Raw NDMI values were additionally averaged by year across all 12 tree-ring isotope sampling locations at SOS for comparison to RWI and $\Delta^{13}C$ chronologies, separately and combined.

2.6 Statistical Analyses

$\Delta^{13}C$ chronologies from SOS were detrended using a 100-year spline to isolate inter-annual to decadal climate trends from low-frequency variation that could arise due to changes in competition, tree height, or rooting depth. Residual isotope series were then multiplied by the mean isotopic value from each core to obtain a pre-whitened isotope series without autocorrelation for each tree. Ring width chronologies from all ponderosa pine sites were detrended separately using a negative exponential spline first to remove the biological growth signal, then with a spline length set to 66% of the time-series length to isolate climate trends. Both live and recently dead trees were combined at sites where both were sampled (SOS and SNF). All detrending was conducted using ARSTAN software (Cook and Krusick 2014). Ring width chronologies and seasonal climate data were similarly pre-whitened to remove autocorrelation and long-term trends, and to highlight interannual variation. This process of detrending and pre-whitening chronologies removes long-term trends and autocorrelation to help ensure that 1) regression analyses of these time-series data had persistence removed so that inter-annual observations would be independent and statistical inferences robust, 2) changes in the explanatory power between two variables over time were not due to shifts in the long-term trends in climate or tree-ring variables, or both in tandem, and 3) no large shifts in autocorrelation occurred over time. We then conducted 35-year running (or moving-window) multiple regression analyses comparing $\Delta^{13}C$ and RWI to summer PDSI, seasonal precipitation, and vapor pressure deficit (VPD) for the years 1900-2016. These 35-year running multiple regressions were performed for RWI vs. PDSI at all sites whereas a latewood $\Delta^{13}C$ chronology spanning this entire period was only available for SOS.

3. Results

3.1 Spatial representativeness of regional drought responses

Our hypothesized EWS include tree-ring metrics that were predictive of whether or not a site underwent widespread forest mortality following the 2012-2015 CA drought. Soaproot Saddle, our primary sampling site, was centrally located within the most severe band of tree mortality in low- to mid-elevation dry mixed-conifer forests of the Sierra Nevada Mountains (**Figure 1**). Inter-annual variability in raw NDMI for grid cells corresponding to tree sampling locations was strongly related to pre-whitened ponderosa pine RWI, $\Delta^{13}C$, and a combination of both over the period 1984-2014 – this is prior to when NDMI started to reflect post-mortality forest canopy desiccation as shown by the NDMI outliers for 2015 and 2016 (**Figure 2**).

3.2 RWI and $\Delta^{13}C$ sensitivity to hydroclimate variables

For SOS, our primary sampling site, regression analyses of drought (summer PDSI) against tree growth (RWI) and latewood $\Delta^{13}C$ showed that summer PDSI values explained at least three-fold more variation in growth and $\Delta^{13}C$ over recent decades compared to the early 1900's (**Figure 3a**). A 35-year moving window length was used to highlight shifts in hydroclimate sensitivity to long-term warming across this region that are not as apparent when using progressively shorter window lengths. This is due to the fact that (1) shorter window lengths result in smaller sample sizes, and (2) that longer moving window lengths more effectively smooth out tree responses and decadal-scale fluctuations in climate (**Figure S1**). We emphasize that PDSI, RWI, and $\Delta^{13}C$ time series were pre-whitened prior to regression analyses to minimize the influence of long-term trends and autocorrelation (see Methods). These increased linkages between PDSI and either RWI or $\Delta^{13}C$ (**Figure 3a**) roughly parallel the long-term decline in PDSI (where negative PDSI values indicate dry conditions) and increase in the number of cold-season growing degree days (>5°C) (**Figure 3b**), indicating a substantial lengthening of the growing season and more frequent or sustained drought conditions. When we examined the NPH index over the past ~100 years, we found that increased precipitation variability in the Sierra Nevada Mountain region and its association with the NPH characterized much of the 20th century (**Figure 3c**). During the CA drought, temperatures peaked at 3.4 to 5.7 standard deviations (SD) above the mean in 2014 and were persistently high; temperatures from the spring of 2013 through the spring of 2015 ranged between 2.0 and 2.9 SD above the mean, depending on the reference period (**Figure 4A-C**). In combination with low precipitation (**Figure 4D-F**), these extreme temperatures made this drought event particularly severe.

A previous investigation of tree-ring growth and $\Delta^{13}C$ at SOS found the strongest responses to PDSI rather than other meteorological or hydroclimate variables (Keen et al. 2020). However, we note that tree-ring metrics also responded to other important drivers of hydroclimate including precipitation and vapor pressure deficit (VPD). Based on 35-year running regressions, spring VPD has become an increasingly important driver of $\Delta^{13}C$ across the entire time period, while $\Delta^{13}C$ sensitivity to summer VPD showed no long-term trends (**Figure S2a-b**). Sensitivity of $\Delta^{13}C$ to spring precipitation rose steadily until approximately 1975, when winter and summer conditions became increasingly influential (Figure S2c-d). Tree growth showed no response to summer precipitation over this time period, but sensitivity of growth to spring VPD increased modestly over the past century (**Figure S3a-d**).

3.3 Applicability of results to additional sites

To assess the ability to use increasing RWI and $\Delta^{13}C$ sensitivity to PDSI as EWS for drought-related mortality in dry mixed-conifer forests, we employed data from six additional ponderosa pine-dominated sites that experienced severe climatic moisture deficits during the CA drought. Century-long latewood $\Delta^{13}C$ chronologies were not available at these sites, so we compared RWI responses to PDSI over the last century. The two locations with the highest mortality rates were SOS and SNF – both of which are located on the western slope of the central Sierra Nevada Mountains that experienced particularly severe drought conditions (**Figure 1a**). These two sites showed a clear, sustained increase in sensitivity of RWI to PDSI over the past century (**Figure 5a-b**), whereas sites that experienced less mortality following the drought event did not have sustained high R^2 values leading up to the CA drought (**Figure 5c-g**). Across all sites (including SOS), the long-term mean growing season climatic moisture deficit (CMD) was strongly related to RWI responses to PDSI leading up to, and including, the California drought (**Figure 5H**). Based on these results, we propose EWS of increased susceptibility to drought-related forest mortality occur when there is a long-term increase in RWI variation explained by PDSI above the threshold R^2 value of 0.4 (EWS 1) or a long-term increase in $\Delta^{13}C$ variation explained by PDSI above the threshold R^2 value of 0.5 (EWS 2) (**Table 1**).

4. Discussion

4.1 Increasing hydroclimate sensitivity as an EWS for drought-related forest mortality

We observed increasing sensitivity of tree-ring variables to hydroclimate prior to drought-related forest mortality at sites where recent drought impacts were most severe. We propose that EWS of impending drought-related mortality events can be tied to emergent, non-stationary tree-ring sensitivity to climate (after Peltier and Ogle 2020) that are initially identifiable based on increasing R^2 of tree-ring variables vs. hydroclimate above a certain threshold (EWS 1 and 2; **Table 1**; **Figure 6**). Previous studies have proposed using declining forest productivity (Rogers et al. 2018; boreal forest) or increased RWI variance in dead trees (i.e., trees that would eventually die, if sampled prior to a mortality event) versus those that were able to survive a mortality event (Cailleret et al. 2019). At SOS in the central Sierra Nevada Mountains, overstory trees displayed increasing growth for decades leading up to the CA drought (Keen et al. 2020), so EWS based on growth rates or productivity likely would not have been applicable for this region. Further, we tested whether amplified population-level variance of inter-annual RWI and/or $\Delta^{13}C$ was apparent leading up to the drought event and predictive of high levels of mortality but found increased variance even at sites that experienced relatively low mortality (**Figure S4**). Overall, this suggests that increasing RWI variance can contribute to increasing R^2 between tree-ring metrics and hydroclimate variables (EWS 1 and 2; **Table 1; Figure 6, S5**), but represents a less reliable metric on which to base EWS compared to increasing RWI and/or $\Delta^{13}C$ sensitivity to hydroclimate.

At Soaproot Saddle, increased hydroclimate variability was likely the main driver of the increasing sensitivity of RWI and $\Delta^{13}C$ to PDSI. Trees at this site displayed increasing growth (Keen et al. 2020) and no declines in raw $\Delta^{13}C$ of individual trees (*data not shown*) in the decades preceding the mortality event. However, it is likely that competition was also a contributing factor since basal area at this site averaged 33 m^2 ha^{-1}. Voelker et al. (2019) identified 25 m^2 ha^{-1} as the point at which increasing drought stress is initiated in ponderosa pine forests of central Oregon, which are generally cooler and wetter than Soaproot Saddle and likely able to support greater basal area, on average. Increasing hydroclimate variability and increased competition for soil water, therefore, were likely both factors that contributed to increasing hydroclimate sensitivity of RWI and $\Delta^{13}C$ (EWS 1 and 2; **Table 1**) at Soaproot Saddle. The detection of EWS 1 and 2 in the decades preceding the CA drought could have provided a set of noteworthy, clear, and complementary indicators of a systemic shift in forest-climate behavior. Our results suggest that the forests at Soaproot Saddle (and the nearby Sierra National Forest site) had reached a threshold whereby they were under much greater threat of a large-scale mortality event (**Figure 6e-f**). Indeed, widespread forest mortality throughout much of the Sierra Nevada Mountains occurred during and following the CA drought (Stephenson et al. 2019), including widespread ponderosa pine mortality due to the western pine beetle outbreak (Fettig et al. 2019; Pile et al. 2019). This threat likely could have been reduced substantially only through large-scale, physical changes to the system, such as long-term climate cooling or mechanical thinning to reduce competition for soil water.

4.2 Variation in hydroclimate sensitivity by site

RWI responses to PDSI across the six additional sites largely reinforced the RWI responses demonstrated at Soaproot Saddle. In addition, there are intriguing nuances to these results that provide lessons for interpreting these responses as EWS. The RWI response to PDSI at the HIR site showed one of the most dramatic increases in R^2, which consistently exceeded 0.4 since ~1980 – however, interstate highway 80 was built immediately adjacent to this site in 1963 and could have resulted in local increases in tropospheric ozone that could potentially have modified stomatal control of water loss (Wilkinson and Davies 2010) and thereby increased ring-width responses to PDSI. At this same site, the trees also displayed a decline in growth response to PDSI over recent decades following the Martis fire in June 2001 that killed many trees across >5800 ha encompassing the site (**Figure 5c**). This presumably reduced competition for soil water, which may have buffered against drought stress or contributed to host trees being more spread out. At the nearby TRS site, there was an even more dramatic decline in RWI hydroclimate sensitivity following a thinning event in the late 1990's (**Figure 5e**; as determined by the presence of stumps at the site and a subsequent growth release of these trees relative to other ponderosa pine sites in the region; S. Voelker, *unpublished analysis*). Therefore, trees at HIR and TRS exemplify how reduced competition for water following fire or thinning, respectively, can moderate growth responsiveness to PDSI, which likely conveyed greater resistance to drought stress during the CA drought.

The Lake Tahoe Basin, which includes the HIR, TRS, and TCR sites, largely escaped widespread mortality during the CA drought, but the RWI responses to PDSI at the HIR and TRS sites suggest that this region may be at risk of future drought-related mortality events, including those due to bark beetles, if basal area continues to increase. In contrast, on the windward side of the Sierra Nevada crest, trees at the FUC site (**Figure 1**) displayed only modest increases in RWI sensitivity to PDSI (**Figure 5g-h**), which suggests that this wetter region may be comparatively buffered from drought-related tree mortality. Finally, the wettest region investigated was at the KEW site in central Oregon, where RWI response to PDSI was consistently lower than all California sites, perhaps driven in part by repeated defoliation events at the site (**Figure 5f**). Since $\Delta^{13}C$ is not as strongly impacted by defoliation compared to RWI, it is worth nothing that running R^2 values of $\Delta^{13}C$ *vs*. PDSI reached $R^2 = 0.5$ during the 1930's Dust Bowl and approached this level again more recently at the KEW site (**Figure S6**). Hence, the sensitivity of $\Delta^{13}C$ to PDSI, but lack thereof for RWI, highlights the utility of using multiple complementary EWS in case the sensitivity of one metric or one locality has been modified by disturbance or other environmental changes.

4.3 Spatial representativeness of EWS 1 and 2

Remote-sensing and/or modeling-based metrics can provide continuous spatial coverage of forest conditions, but forecasting forest dieback based on tree-ring EWS does not yet have a known spatial scale. Since tree-ring based EWS are in their infancy, there is also substantial uncertainty in the upper limits for the spatial scale at which tree-ring EWS may be useful. Although climate responsiveness of many forests was similar across scales of 400 km or greater (**Figure S7**), the sites we investigated in northern California that did not display strong mortality (**Figure 5**) were about 250 km away and the most concentrated forest mortality was located within 150 km north and south of SOS (**Figure 1**). Given this coarse spatial information, we initially hypothesized that EWS would be relevant for similar forest types at distances of up to 200 km, but increasingly reliable at shorter distances. The so-called first law of geographic proximity dictates that forests nearer to that which EWS have been detected will be at an increased likelihood of dieback compared to those further away. However, substantial spatial variability will be superimposed upon this general rule by sub-regional meteorological drought conditions (e.g., Williams et al. 2015), as well as stand-level differences in competition stress and the concentration of host species in drought susceptibility (Voelker et al. 2019; Keen et al. 2020). While this general rule must be modified by a number of local factors including forest type, stand density, bark beetle host tree density, regional-scale planning that can effectively integrate local spatial (i.e., remote sensing) and temporal (i.e., tree-rings) records will be best equipped alongside EWS to mitigate the effects of future droughts and associated bark beetle outbreaks.

5. Conclusions and Implications

As the warming climate continues to cause chronic drought stress to grip much of the western United States (Williams et al. 2020), drought conditions have explained a large share of regional pulses in forest disturbance events such as bark beetle outbreaks and heightened wildfire activity (Raffa et al. 2008; Williams et al. 2013; Kolb et al. 2019; Higuera and Abatzoglou 2020). The 2020 Creek Fire in California is a recent example – this fire was the largest single-source fire in California's history and burned much of the area surrounding the SOS and SNF sites. A large portion of this area was densely populated by dead trees, predominantly ponderosa pine, following the CA drought and associated western pine beetle outbreak. To help avoid this scenario elsewhere in the future, we have described and demonstrated two EWS that we propose can be used to identify shifting patterns in tree hydroclimate sensitivity that confer an increased likelihood of widespread mortality during episodic drought events: increasing sensitivity of (1) RWI and (2) $\Delta^{13}C$ to PDSI or a related hydroclimate variable, where sensitivity is defined as increasing R^2 of a tree-ring variable vs. PDSI through time (**Table 1**).

If foreknowledge provided by these EWS had been identified 10 or 20 years earlier, some of the > 150 million tree deaths in California over the past five years (USDA Forest Service 2019) could likely have been mitigated via thinning, prescribed burning, or via management of wildfire ignitions where feasible. Although analysis of tree-ring $\Delta^{13}C$ can be costly and time-intensive, measurement of tree-growth (RWI) is typically simpler, less costly, and likely more feasible for collection at a large scale for use in forest monitoring. However, we note that the use of multiple tree-ring properties when assessing EWS of forest mortality is preferable and reduces the chances of missing signs of susceptibility or detecting a false positive. In the face of projected warming and increasing hydrological extremes for forests in California and rest of the western United States (Yoon et al. 2015; Williams et al. 2020; Martin et al. 2020), wider deployment of tree-ring based EWS, in concert with remote sensing of vegetation moisture deficits, should provide more accurate forecasting of where forest management actions can most effectively mitigate the likelihood of future warming- and drought-driven forest mortality events.

Acknowledgments

We thank the Southern Sierra Critical Zone Observatory for providing access to the Soaproot Saddle field site. We would also like to thank Beverly Bulaon from the Forest Service, Forest Health Protection and Erin Stacy from the CZO for their substantial help with sampling and selection of field sites. We also thank Ramzi Touchan and Eylon Shamir for contributing ring-width data from two sites as well as comments and photographs of the trees and stands sampled. We acknowledge funding support from the National Science Foundation (NSF-MSB-1241286 and NSF-P2C2-1903721) and from USDA Forest Service Forest Health Protection (EM-18-WC-03).

References

1. Adams, H.D., Macalady, A.K., Breshears, D.D., Allen, C.D., Stephenson, N.L., Saleska, S.R., Huxman, T.E., & McDowell, N.G. (2010) Climate-induced tree mortality: earth system consequences. Eos, 91, 153–154
2. Allen, C.D., Macalady, A.K., Chenchouni, H., Bachelet, D., McDowell, N., Vennetier, M., Kitzberger, T., Rigling, A., Breshears, D.D., Hogg, E.H., Gonzalez, P., Fensham, R., Zhang, Z., Castro, J., Demidova, N., Lim, J.H., Allard, G., Running, S.W., Semerci, A., & Cobb, N. (2010) A global overview of drought and heat-induced tree mortality reveals emerging climate change risks for forests. *Forest Ecology and Management*, 259, 660-684
3. Anderegg, W.R., Kane, J.M. & Anderegg, L.D. (2013) Consequences of widespread tree mortality triggered by drought and temperature stress. *Nature Climate Change*, 3, 30-36
4. Asner, G.P., Martin R.E., Anderson, C.B. & Knapp, D.E. (2015) Quantifying forest canopy traits: Imaging spectroscopy versus field survey *Remote Sensing of Environment,* 158, 15-27
5. Black, B.A., van der Sleen, P., Di Lorenzo, E., Griffin, D., Sydeman, W.J., Dunham, J.B., Rykaczewski, R.R., García-Reyes, M., Safeeq, M., Arismendi, I. & Bograd, S.J. (2018). Rising synchrony controls western North American ecosystems. *Global Change Biology*, *24*, 2305-2314.
6. Brodrick, P.G. & Asner, G.P. (2017) Remotely sensed predictors of conifer tree mortality during severe drought. *Environmental Research Letters*, 12, 115013.
7. Cailleret, M., Dakos, V., Jansen, S., Robert, E.M., Aakala, T., Amoroso, M.M., Antos, J.A., Bigler, C., Bugmann, H., Caccianiga, M. & Camarero, J.J., 2019. Early-warning signals of individual tree mortality based on annual radial growth. *Frontiers in plant science*, *9*, 1964.
8. Cook, E.R., & Krusic, P.J. (2014) ARSTAN version 44h3: A tree-ring standardization program based on detrending and autoregressive time series modeling, with interactive graphics. Tree-Ring Laboratory, Lamont-Doherty Earth Observatory of Columbia University, Palisades, New York, USA
9. Douglass, A.E. 1914. Method of estimating rainfall by the growth of trees. *Bulletin of the American Geographic Society*, 46, 323-325.
10. Ehleringer, J.R., Hall, A.E., & Farquhar, GD (1993) Stable Isotopes and Plant Carbon–Water Relations. Academic Press, New York
11. Farquhar, G.D., O'Leary, M.H., & Berry, J.A. (1982) On the relationship between carbon isotope discrimination and intercellular carbon dioxide concentration in leaves. *Australian Journal of Plant Physiology*, 9, 121–137.
12. Farquhar, G.D., Ehleringer, J.R., & Hubick, K.T. (1989) Carbon isotope discrimination and photosynthesis. *Annual Review of Plant Physiology and Plant Molecular Biology*, 40, 503-537
13. Fettig, C.J., Mortenson, L.A., Bulaon, B.M., & Foulk, P.B. (2019) Tree mortality following drought in the central and southern Sierra Nevada, California, US. *Forest ecology and Management*, 432, 164-78
14. Fritts, H. C. (1976), Tree Rings and Climate, 567 pp., Academic, San Diego, Calif.
15. Gleick, P.H. (1987) Regional Hydrologic Consequences of increases in Atmospheric Carbon Dioxide and other Trace Gases *Climatic Change*, 10, 137–161.
16. Goulden, M.L., & Bales. R.C. (2019) California forest die-off linked to multi-year deep soil drying in 2012–2015 drought. *Nature Geoscience*, 12, 632-637.

17. Goulden, M.L., Anderson, R.G., Bales, R.C., Kelly, A.E., Meadows, M., & Winston, G.C. (2012) Evapotranspiration along an elevation gradient in California's Sierra Nevada. *Journal of Geophysical Research: Biogeosciences*, 117(G3).
18. Griffin, D. & Anchukaitis, K.J. (2014) How unusual is the 2012-2014 California drought? *Geophysical Research Letters,* 41, 9017–9023
19. Higuera, P.E., & Abatzoglou, J.T. (2020) Record-setting climate enabled the extraordinary 2020 fire season in the western United States. Global Change Biology.
20. Kagawa, A., Sugimoto, A., & Maximov, T.C. (2006) $^{13}CO_2$ pulse-labelling of photoassimilates reveals carbon allocation within and between tree rings *Plant, Cell & Environment*, 29, 1571-1584.
21. Keen, R.M., Voelker, S.L., Bentz, B.J., Wang, S.Y.S., & Ferrell, R. (2020) Stronger influence of growth rate than severity of drought stress on mortality of large ponderosa pines during the 2012–2015 California drought. Oecologia, 194(3), pp.359-370.
22. Knowles, N., & Cayan, D. (2004) Elevational Dependence of Projected hydrologic changes in the San Francisco estuary and watershed. *Climatic Change,* 62, 319–336.
23. Kolb, T.E., Grady, K.C., McEttrick, M.P., & Herrero, A. (2016) Local-scale drought adaptation of ponderosa pine seedlings at habitat ecotones. *Forest Science*, 62, 641-651
24. Kolb, T., Keefover-Ring, K., Burr, S.J., Hofstetter, R., Gaylord, M. & Raffa, K.F. (2019) Drought-Mediated Changes in Tree Physiological Processes Weaken Tree Defenses to Bark Beetle Attack. *Journal of Chemical Ecology*, 45, 888-900.
25. Kukal, M.S., & Irmak, S. (2018) US Agro-Climate in 20th Century: Growing Degree Days, First and Last Frost, Growing Season Length, and Impacts on Crop Yields. *Scientific Reports*, 8, 6977.
26. Laumer, W., Andreu, L., Helle, G., Schleser, G.H., Wieloch, T., & Wissel, H. (2009) A novel approach for the homogenization of cellulose to use micro-amounts for stable isotope analysis. *Rapid Communications in Mass Spectrometry*, 23,1934-1940
27. Leavitt, S.W., & Danzer, S.R. (1993) Method for batch processing small wood samples to holocellulose for stable isotope analysis. *Analytical Chemistry* 65, 87-89
28. Leavitt, S.W., Woodhouse, C.A., Castro, C.L., Wright, W.E., Meko, D.M., Touchan, R., Griffin, D., & Ciancarelli, B. (2011) The North American monsoon in the US Southwest: Potential for investigation with tree-ring carbon isotopes. *Quaternary International*, 235, 101–107
29. Liu, Y., Kumar, M., Katul, G. G., & Porporato, A. (2019). Reduced resilience as an early warning signal of forest mortality. *Nature Climate Change*, 9, 880-885.
30. Luo, L., Apps, D., Arcand, S., Xu, H., Pan, M., & Hoerling, M. (2017) Contribution of temperature and precipitation anomalies to the California drought during 2012–2015. *Geophysical Research Letters*, 44, 3184-3192.
31. Martin, J.T., Pederson, G.T., Woodhouse, C.A., Cook, E.R., McCabe, G.J., Anchukaitis, K.J., Wise, E.K., Erger, P.J., Dolan, L., McGuire, M., & Gangopadhyay, S. (2020) Increased drought severity tracks warming in the United States' largest river basin. *Proceedings of the National Academy of Sciences*, 117, 11328-11336.
32. McCarroll, D., & Loader, N.J. (2004) Stable isotopes in tree rings. *Quaternary Science Reviews*, 23, 771-801
33. Millar, C. I., & Stephenson, N.L. (2015) Temperate forest health in an era of emerging megadisturbance. *Science*, 349, 823-826.

34. Morris, J.L., Cottrell, S., Fettig, C.J., DeRose, R.J., Mattor, K.M., Carter, V.A., Clear, J., Clement, J., Hansen, W.D., Hicke, J.A. and Higuera, P.E., 2018. Bark beetles as agents of change in social–ecological systems. *Frontiers in Ecology and the Environment*, 16, S34-S43.
35. Mote, P.W., Hamlet, A.F., Clark, M.P., & Lettenmaier, D.P. (2005) Declining mountain snow pack in western North America *Bulletin of the American Meteorological Society*, 86, 39-49.
36. North, M., Hurteau, M., Fiegener, R., & Barbour, M. (2005) Influence of fire and El Nino on tree recruitment by species in Sierran mixed conifer. Forest Science, 51, 187-197.
37. Parsons, D.J., & DeBenedetti, S.H. (1979) Impact of fire suppression on a mixed-conifer forest. *Forest Ecology and Management*, 2, 21-33
38. Peltier, D.M., & Ogle, K. (2020) Tree growth sensitivity to climate is temporally variable. *Ecology Letters*, 23, 1561-1572.
39. Pile, L.S., Meyer, M.D., Rojos, R., Roe, O., & Smith, M.T. (2019) Drought impacts and compounding mortality of forest trees in the southern Sierra Nevada. *Forests*, 10, 237.
40. Raffa, K.F., Aukema, B.H., Bentz, B.J., Carroll, A.L., Hicke, J.A., Turner, M.G., & Romme, W.H. (2008) Cross-scale drivers of natural disturbances prone to anthropogenic amplification: the dynamics of bark beetle eruptions. *BioScience*, 58, 501-517
41. Reed, C.C., & Hood, S.M. (2020) Few generalizable patterns of tree-level mortality during extreme drought and concurrent bark beetle outbreaks. *Science of the Total Environment*, 750, 141306.
42. Rinne, K.T., Boettger, T., Loader, N.J., Robertson, I., Switsur V.R., & Waterhouse, J.S. (2005) On the purification of a-cellulose from resinous wood for stable isotope (H, C and O) analysis. *Chemical Geology*, 222, 75-82
43. Roden, J.S., & Ehleringer J.R. (2007) Summer precipitation influences the stable oxygen and carbon isotopic composition of tree-ring cellulose in Pinus ponderosa. *Tree Physiology*, 27, 491–501
44. Rogers, B.M., Solvik, K., Hogg, E.H., Ju, J., Masek, J.G., Michaelian, M., Berner, L.T., & Goetz, S.J. (2018) Detecting early warning signals of tree mortality in boreal North America using multiscale satellite data. *Global Change Biology*, *24*, 2284-2304.
45. Schook, D.M., Friedman, J.M., Stricker, C.A., Csank, A.Z., & Cooper, D.J. (2020) Short- and long-term responses of riparian cottonwoods (Populus spp.) to flow diversion: Analysis of tree-ring radial growth and stable carbon isotopes. *Science of the Total Environment*, 735, 139523.
46. Shamir, E., Meko, D., Touchan, R., Lepley, K.S., Campbell, R., Kaliff, R.N., & Georgakakos, K.P. (2020) Snowpack-and Soil Water Content-Related Hydrologic Indices and Their Association With Radial Growth of Conifers in the Sierra Nevada, California. *Journal of Geophysical Research: Biogeosciences*, 125, e2019JG005331.
47. Sperry, J.S., Venturas, M.D., Todd, H.N., Trugman, A.T., Anderegg, W.R., Wang, Y., & Tai, X. (2019). The impact of rising CO_2 and acclimation on the response of US forests to global warming. *Proceedings of the National Academy of Sciences*, *116*, 25734-25744.
48. Stephens, S.L., Lydersen, J.M., Collins, B.M., Fry, D.L., & Meyer, M.D. (2015) Historical and current landscape-scale ponderosa pine and mixed conifer forest structure in the Southern Sierra Nevada. *Ecosphere* 6, 1-63
49. Stephenson, N.L., Das, A.J., Ampersee, N.J., Bulaon, B.M., & Yee, J.L. (2019) Which trees die during drought? The key role of insect host-tree selection. Journal of Ecology, 107(5), pp.2383-2401.

50. Stewart, I.T., Cayan, D.R., & Dettinger, M.D. (2004) Changes in snowmelt runoff timing in western North America under a business as usual climate change scenario. *Climatic Change*, 62, 217-32
51. Stokes, M.A., & Smiley, T. (1968) An Introduction to Tree-Ring Dating. University of Chicago Press, Chicago
52. Szejner, P., Wright, W.E., Babst, F., Belmecheri, S., Trouet, V., Leavitt, S..W, Ehleringer, J.R., & Monson, R.K. (2016) Latitudinal gradients in tree-ring stable carbon and oxygen isotopes reveal differential climate influences of the North American Monsoon system. *Journal of Geophysical Research: Biogeosciences*, 121, 1978-1991.
53. Trumbore, S., Brando, P. & Hartmann, H. (2015) Forest health and global change. Science, 349, 814-818.
54. U.S. Forest Service Pacific Southwest Region Forest Health Protection Aerial Detection Survey. (2019). Available at: https://www.fs.usda.gov/detail/r5/forest-grasslandhealth/?cid=fsbdev3_046696.
55. Van de Water, K.M., & Safford, H.D. (2011) A summary of fire frequency estimates for California vegetation before Euro-American settlement. *Fire Ecology*, 7, 26-58
56. Van Mantgem, P.J., Stephenson, N.L., Byrne, J.C., Daniels, L.D., Franklin, J.F., Fule, P.Z., Harmon, M.E., Larson, A.J., Smith, J.M., Taylor, A.H., & Veblen, T.T. (2009) Widespread increase of tree mortality rates in the Western United States. *Science*, 323, 521-524.
57. Voelker, S.L., Merschel, A.G., Meinzer, F.C., Ulrich, D.E., Spies, T.A., & Still, C.J. (2019) Fire deficits have increased drought sensitivity in dry conifer forests: Fire frequency and tree-ring carbon isotope evidence from Central Oregon. *Global Change Biology*, 25, 1247-1262.
58. Wang, T., Hamann, A., Spittlehouse, D., & Carroll, C. (2016) Locally downscaled and spatially customizable climate data for historical and future periods for North America. *PloS one*, 11, e0156720.
59. Wilkinson, S., & Davies, W.J. (2010) Drought, ozone, ABA and ethylene: new insights from cell to plant to community. *Plant, Cell & Environment*, 33, 510-525.
60. Williams, A.P., Allen, C.D., Macalady, A.K., Griffin, D., Woodhouse, C.A., Meko, D.M., Swetnam, T.W., Rauscher, S.A., Seager, R., Grissino-Mayer, H.D., Dean, J.S., Cook, E.R., Gangodagamage, C., Cai, M. McDowell, N.G. (2013) Temperature as a potent driver of regional forest drought stress and tree mortality. *Nature Climate Change*, 3, 292-297
61. Williams, A.P., Cook, E.R., Smerdon, J.E., Cook, B.I., Abatzoglou, J.T., Bolles, K., Baek, S.H., Badger, A.M., & Livneh, B. (2020) Large contribution from anthropogenic warming to an emerging North American megadrought. *Science*, 368, 314-318.
62. Williams, A.P., Seager, R., Abatzoglou, J.T., Cook, B.I., Smerdon, J.E., & Cook, E.R. (2015) Contribution of anthropogenic warming to California drought during 2012–2014. *Geophysical Research Letters*, 4, 819-6828.
63. Xu, C., McDowell, N.G., Fisher, R.A., Wei, L., Sevanto, S., Christoffersen, B.O., Weng, E., & Middleton, R.S. (2019) Increasing impacts of extreme droughts on vegetation productivity under climate change. *Nature Climate Change*, 9, 948-953.
64. Yoon, J-H., Wang, S-Y., Gillies, R.R., Kravitz, B., Hipps L., & Rasch, P.J. (2015) Increasing water cycle extremes in California and in relation to ENSO cycle under global warming. *Nature Communications*, 6, 8657.

Table 1: Characteristics of proposed Early Warning Signals (EWS) 1 and 2.

	EWS mechanism	Time preceding mortality	Forest/species type	Foremost limitations
EWS 1	Long-term increase in RWI variation explained by PDSI sustained above threshold $R^2 > 0.40$	~ 20 years	Dry mixed-conifer forest	Tree-ring data can be time-intensive to collect across landscapes
EWS 2	Long-term increase in $\Delta^{13}C$ variation explained by PDSI sustained above threshold $R^2 > 0.50$	~ 20 years	Dry mixed-conifer forest	Tree-ring data can be time-intensive to collect across landscapes. Isotope data require further preparation and costs.

Figure 1 Sampling locations overlayed on to the difference in Landsat Normalized Difference Moisture Index (δNDMI, after Goulden and Bales 2019) between 2012 and 2016 dry seasons displayed for the Sierra Nevada Mountains and a subset including our primary data collection site at Soaproot Saddle (SOS) (A-B). δNDMI displayed in panels A and B were masked (black) to remove areas that had burned since 1980, were not conifer-dominated forests, had mean annual precipitation of less than 600 mm, or were outside of the Sierra Nevada ecoregion. Sampling locations of trees used for stable isotope measurements at SOS are overlayed on unmasked δNDMI (C).

Figure 2 The dependence of interannual variation in ponderosa pine ring width increment (RWI) Z-scores (A), carbon isotope discrimination ($\Delta^{13}C$) Z-scores (B) or means across both Z-scores (C) to Landsat Normalized Difference Moisture Index (NDMI) centered on the SOS site over the period 1984-2016. The years labelled as 2015 and 2016 are NDMI outliers that were not included in regression relationships because NDMI for these two years was strongly influenced by post-mortality desiccation rather than *in vivo* drought stress.

Figure 3 (A) 35-year running R^2 values from regression analyses comparing $\Delta^{13}C$ (maroon) and RWI (pink) to summer (JJA) PDSI at SOS; note that more negative PDSI values indicate greater moisture deficits. (B) 35-year running average of summed (November-May) growing degree days (GDD; > 5°C) (green) and PDSI (yellow). (C) 35-year running standard deviation in precipitation amounts (mm) (blue) and winter North Pacific High (NPH) geopotential height values (hPa; after Black et al. 2018) (gray). GDD calculations and precipitation were centered on the SOS site, as interpolated by the ClimateNA program (Wang et al. 2016).

Figure 4 Standard deviations (SD) from mean temperatures or precipitation at SOS. Temperatures are depicted at annual (A) and seasonal (3-month) (B) resolution from 1900-2016 or expanded for 2000-2016 (C) with respect to different reference periods. Precipitation data are displayed in the same manner (D-F). Seasons were defined by the following month groupings: Winter = DJF, Spring = MAM, Summer = JJA, Fall = SON.

Figure 5 35-year running R^2 values from regression using summer (JJA) PDSI to predict RWI are plotted for each of seven ponderosa pine sites over the years 1901 to 2015 or 2016 (A-G) (see Fig 1). The most recent four running R^2 values common to all sites, corresponding to 2012-2015, were averaged and plotted against the summed 1961-1990 mean annual climate moisture deficit (H). Climatic moisture deficit values, defined as water year potential evapotranspiration - precipitation were obtained from ClimateNA (Wang et al. 2016). Estimates of site-level forest mortality, represented by the blue to red color scale, were determined using visual assessments of forest mortality from (https://egis.fire.ca.gov/TreeMortalityViewer/) and/or satellite imagery available from Google Earth for the years 2016 and 2017.

Figure 6 Conceptual diagrams depicting increasing tree-ring variance in response to increasing competition for soil water and drought stress following a disrupted disturbance regime (e.g., fire suppression) (A) or increasing hydroclimate variation (B). Under both conditions the explained variation in tree-ring metrics should respond in a nearly logistic curve over time (C-D) and increase the probability of a large-scale mortality event due to drought or insect pests non-linearly (E-F). Each set of response curves includes scenarios demonstrating either hydroclimate sensitive or insensitive responses of a site or tree-ring metric. Mapped onto these response curves and scenarios are Early Warning Signals (EWS) 1 and 2 (see **Table 1**). EWS 1 and 2 are only possible above a threshold R^2 value (horizontal dashed line).

Figure 1

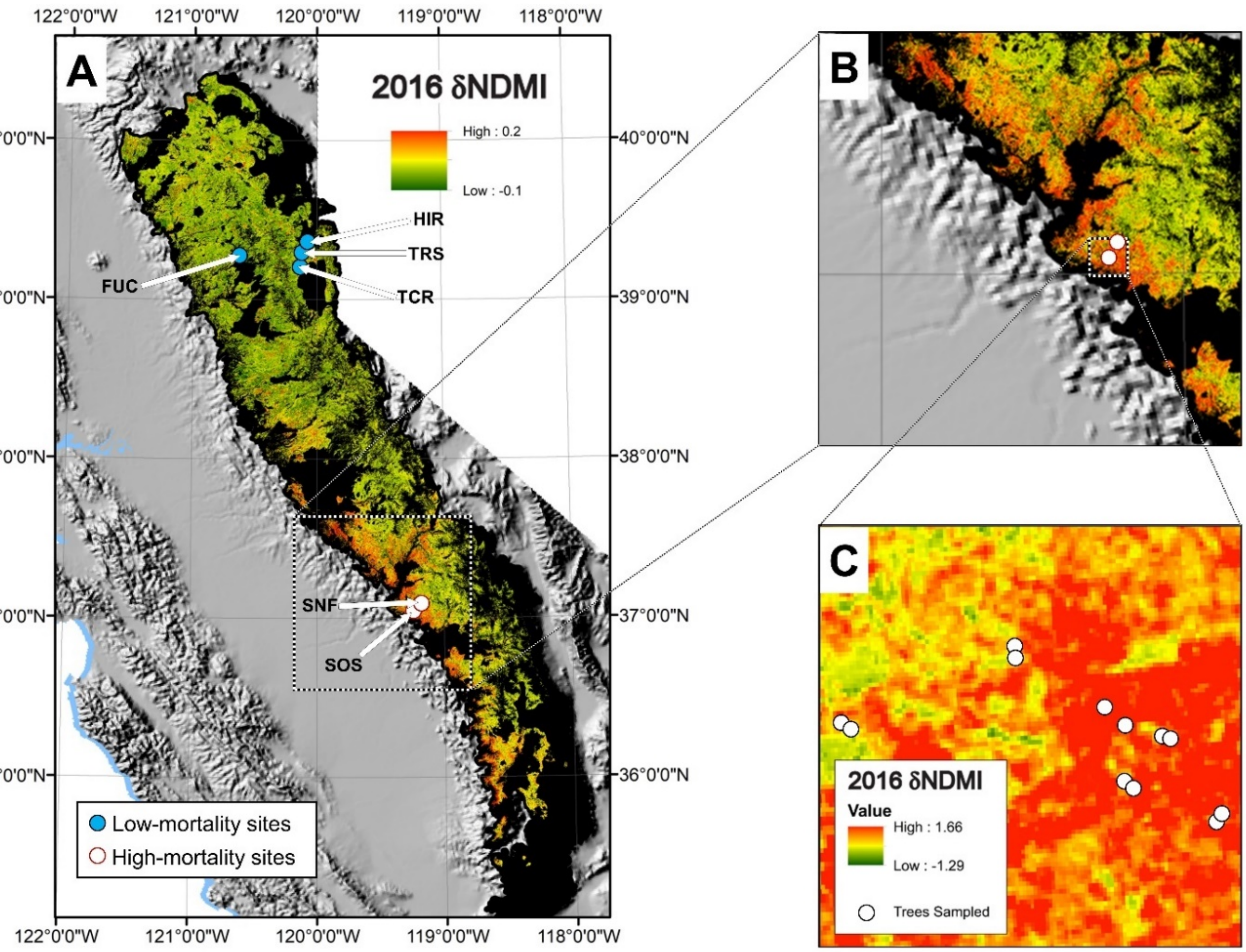
A
2016 δNDMI
High : 0.2
Low : -0.1
HIR
TRS
TCR
FUC
SNF
SOS
Low-mortality sites
High-mortality sites
122°0'0"W
121°0'0"W
120°0'0"W
119°0'0"W
118°0'0"W
40°0'0"N
39°0'0"N
38°0'0"N
37°0'0"N
36°0'0"N
B
C
2016 δNDMI
Value
High : 1.66
Low : -1.29
Trees Sampled

Figure 2

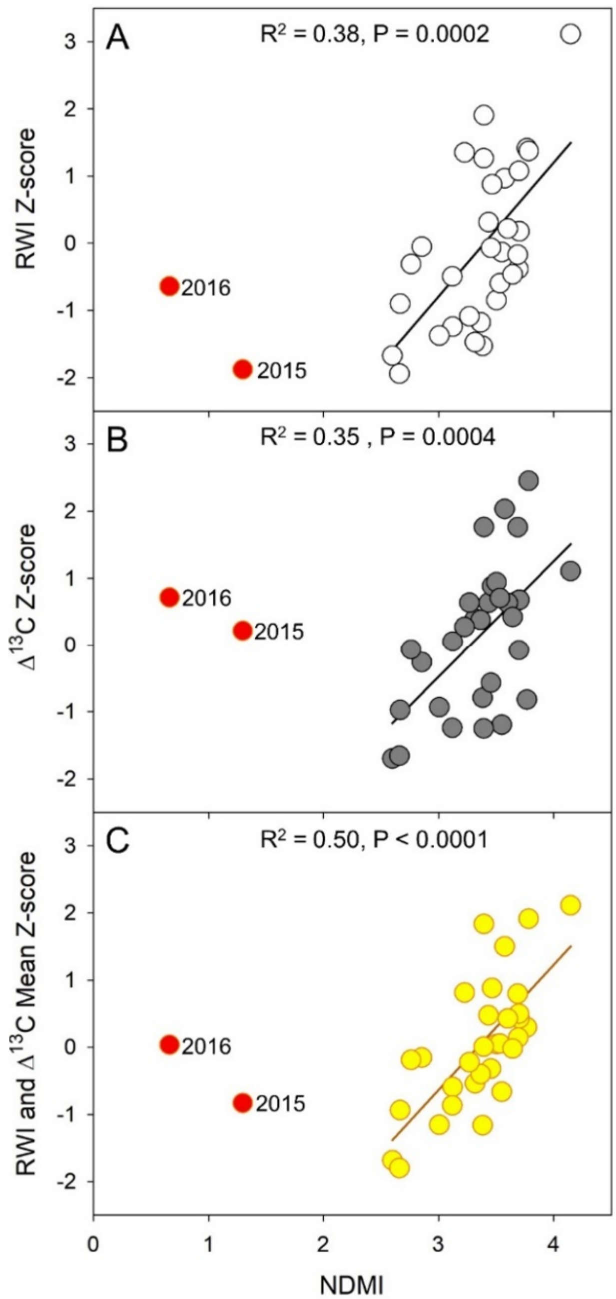

A
R² = 0.38, P = 0.0002
RWI Z-score
2016
2015
B
R² = 0.35 , P = 0.0004
Δ13C Z-score
2016
2015
C
R² = 0.50, P < 0.0001
RWI and Δ13C Mean Z-score
2016
2015
NDMI

Figure 3

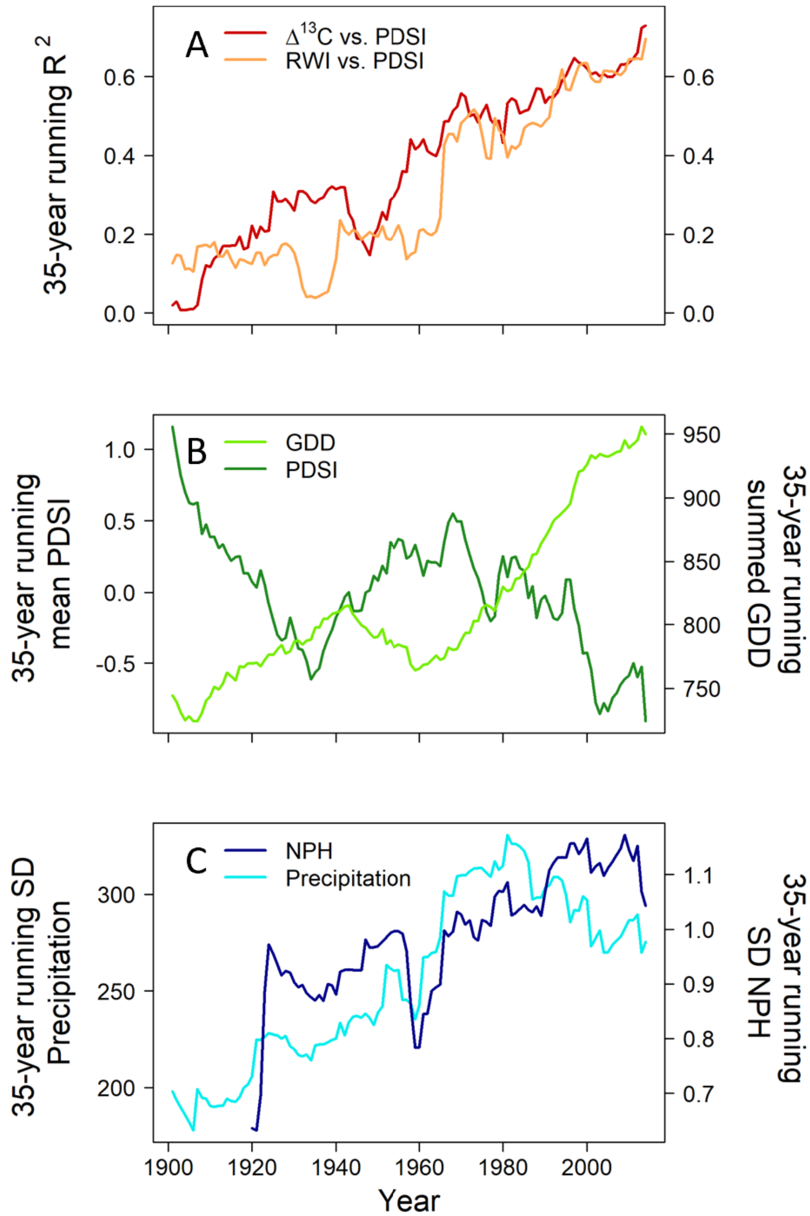
A
Δ^{13}C vs. PDSI
RWI vs. PDSI
35-year running R^2
0.0
0.2
0.4
0.6
B
GDD
PDSI
35-year running mean PDSI
35-year running summed GDD
1.0
0.5
0.0
-0.5
950
900
850
800
750
C
NPH
Precipitation
35-year running SD Precipitation
35-year running SD NPH
300
250
200
1.1
1.0
0.9
0.8
0.7
1900
1920
1940
1960
1980
2000
Year

Figure 4

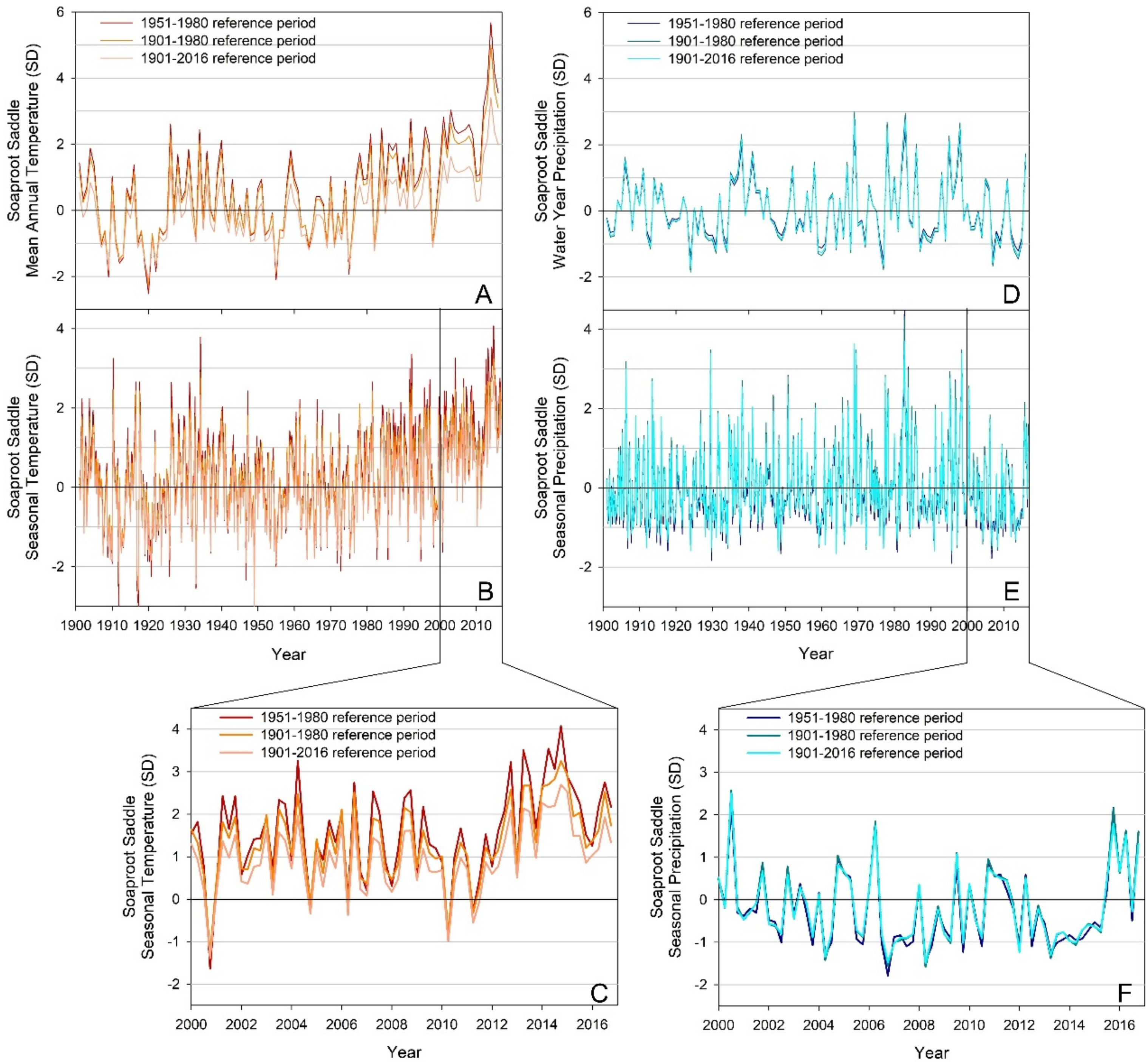
1951-1980 reference period
1901-1980 reference period
1901-2016 reference period
Soaproot Saddle
Mean Annual Temperature (SD)
A
Soaproot Saddle
Water Year Precipitation (SD)
D
Soaproot Saddle
Seasonal Temperature (SD)
B
Soaproot Saddle
Seasonal Precipitation (SD)
E
Year
C
F

Figure 5

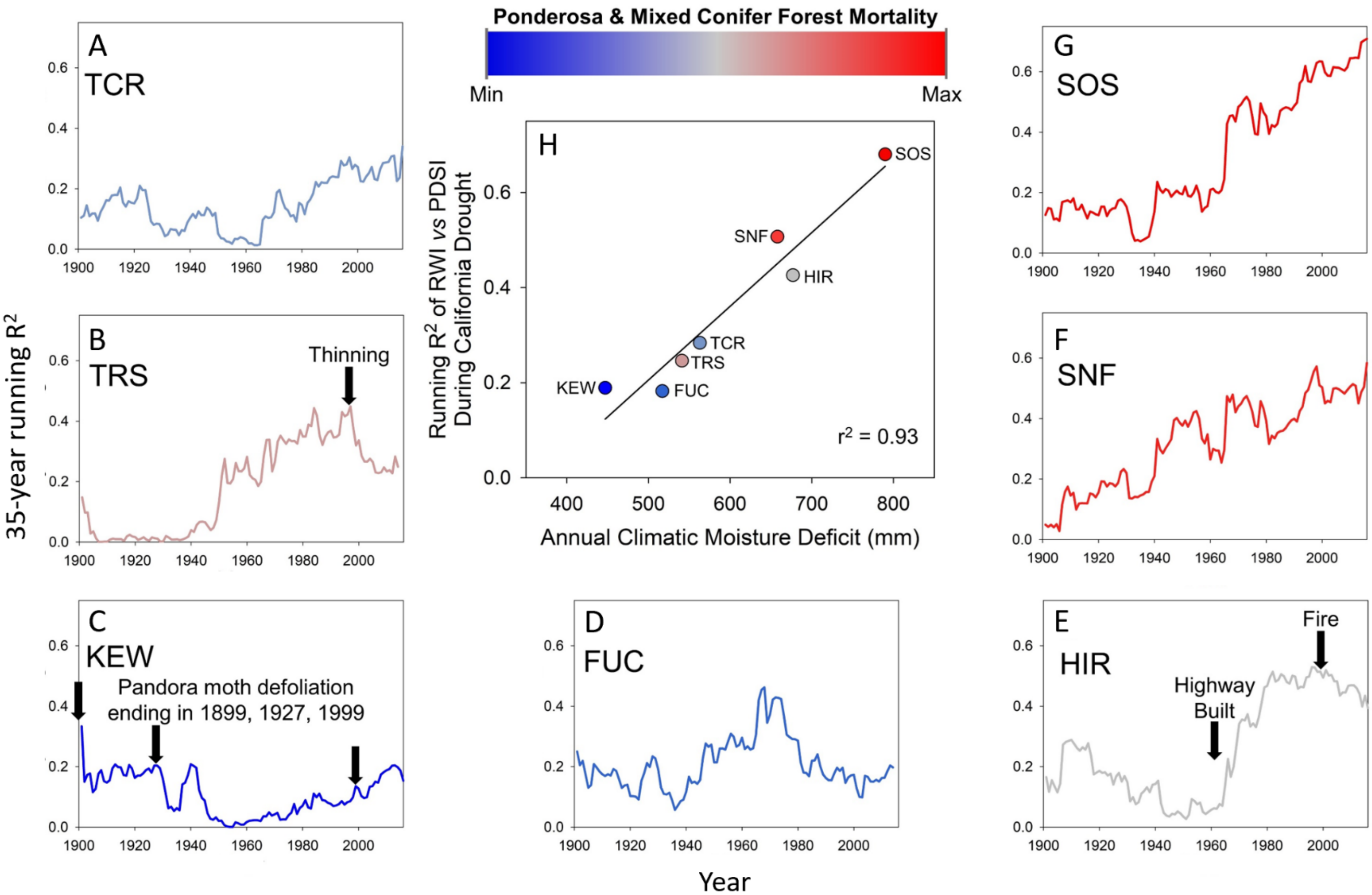
Ponderosa & Mixed Conifer Forest Mortality
Min
Max
A
TCR
B
TRS
Thinning
C
KEW
Pandora moth defoliation
ending in 1899, 1927, 1999
D
FUC
E
HIR
Highway
Built
Fire
F
SNF
G
SOS
H
SOS
SNF
HIR
TCR
TRS
KEW
FUC
r^2 = 0.93
Running R^2 of RWI *vs* PDSI During California Drought
Annual Climatic Moisture Deficit (mm)
35-year running R^2
Year

Figure 6

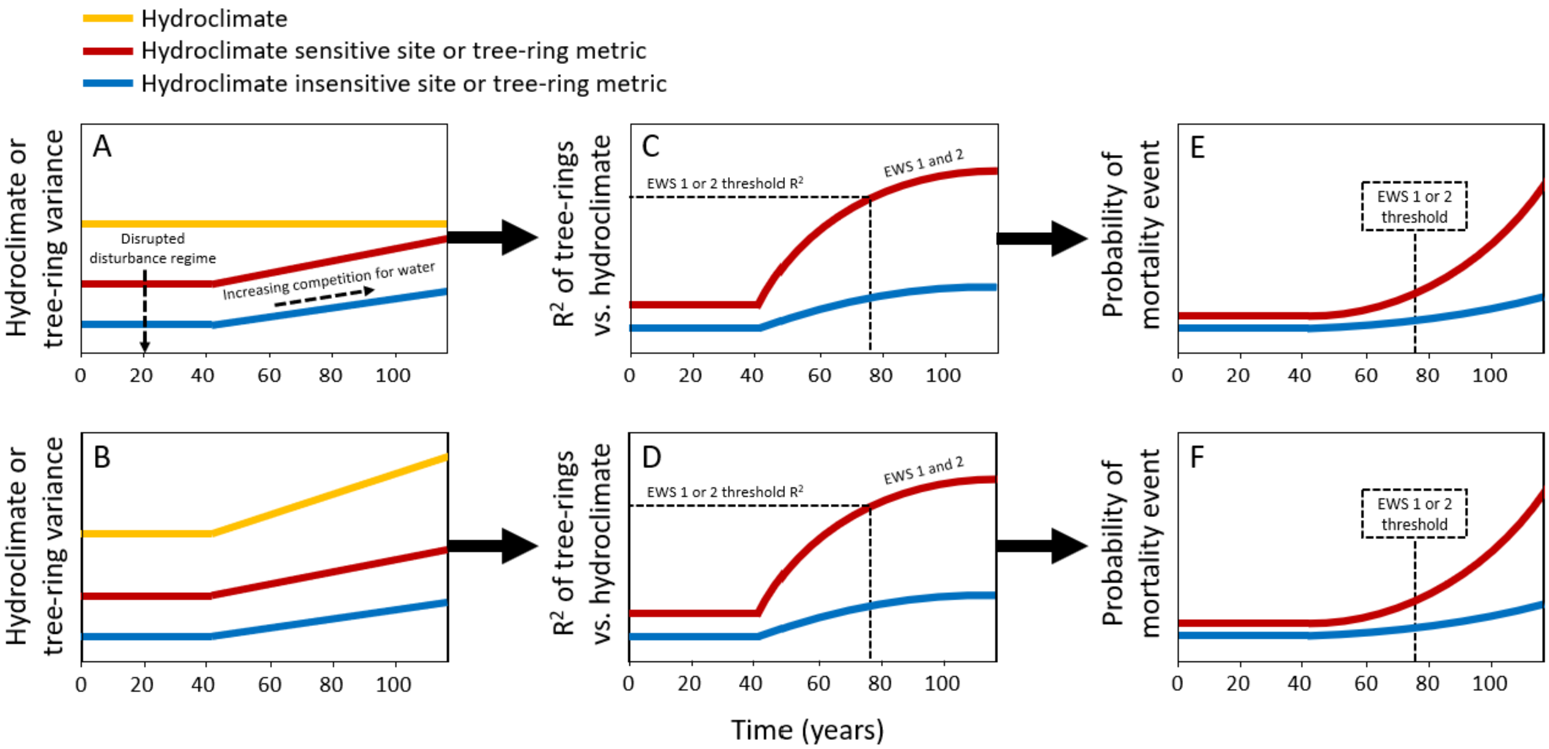

Hydroclimate
Hydroclimate sensitive site or tree-ring metric
Hydroclimate insensitive site or tree-ring metric
Hydroclimate or tree-ring variance
A
Disrupted disturbance regime
Increasing competition for water
B
R² of tree-rings vs. hydroclimate
C
D
EWS 1 or 2 threshold R²
EWS 1 and 2
Probability of mortality event
E
F
EWS 1 or 2 threshold
0
20
40
60
80
100
Time (years)

Supplementary Information for Keen et al. 2021; Changes in tree drought sensitivity provided early warning signals to the California drought and forest mortality event

Supplementary Table S1 – A survey and descriptive characteristics of Early Warning Signals.

Early warning signal mechanism	Source	Time preceding mortality	Forest/Species Types	Foremost Limitations
Remote sensing of canopy water content (CWC)	Brodrick and Asner 2017	1-3 years	Multiple types	% loss in CWC increased above mean value for two years prior to widespread mortality. At Soaproot Saddle % loss in CWC significantly higher than background starting in 2015, 0-2 years before widespread mortality
Remote sensing of CWC	Goulden and Bales 2019	1-3 years	Multiple types, mostly Dry mixed conifer	At Soaproot Saddle NDMI was significantly lower than background starting in 2014, 1-3 years before widespread mortality
Remote sensing of vegetation greenness	Rogers et al. 2018	Up to 24 years	Boreal forests	Detects long-term declines in productivity that may precede episodic mortality in some forest types. Tree growth data at Soaproot Saddle show no decline in productivity prior to the California drought.
Remote sensing of non-photosynthetically active vegetation	Anderegg et al. 2019	4-5 years	Angiosperms that undergo leaf abscission, branch dieback	Remote sensing data is acquired after an inciting drought, so there is no way to mitigate drought severity, only know where tree mortality will be concentrated
Remote sensing of vegetation greenness	Liu et al. 2019	0.5-1.6 years	Dry mixed conifer	A short lead-time of 0.5-1.6 years prior to mortality provides little time to enact management activities that could mitigate the severity of forest dieback
Increasing RWI variance of dead vs surviving trees	Cailleret et al. 2019	~20 years	Many temperate forest types	Need to know which trees will live or die, possible false positive EWS detection when occurring at low levels of tree stress that present low risk of widespread mortality
Long-term increase in RWI variation explained by PDSI sustained above threshold $R^2 > 0.40$	This study, EWS 1	~20 years	Dry mixed conifer forests	Tree-ring data can be time-intensive to collect across landscapes
Long-term increase in $\Delta^{13}C$ variation explained by PDSI sustained above threshold $R^2 > 0.50$	This study, EWS 2	~20 years	Dry mixed conifer forests	Tree-ring data can be time-intensive to collect across landscapes. Isotope data take further preparation and costs

Supplementary Figure S1 – Comparison of running R^2 for $\Delta^{13}C$ vs current and previous year PDSI calculated across time windows of 35-, 25- and 15-years length (top, middle and bottom, respectively). Data near the ends of the moving window relationships progressively shrink to a minimum of N/2+1 years in length, where N = window length.

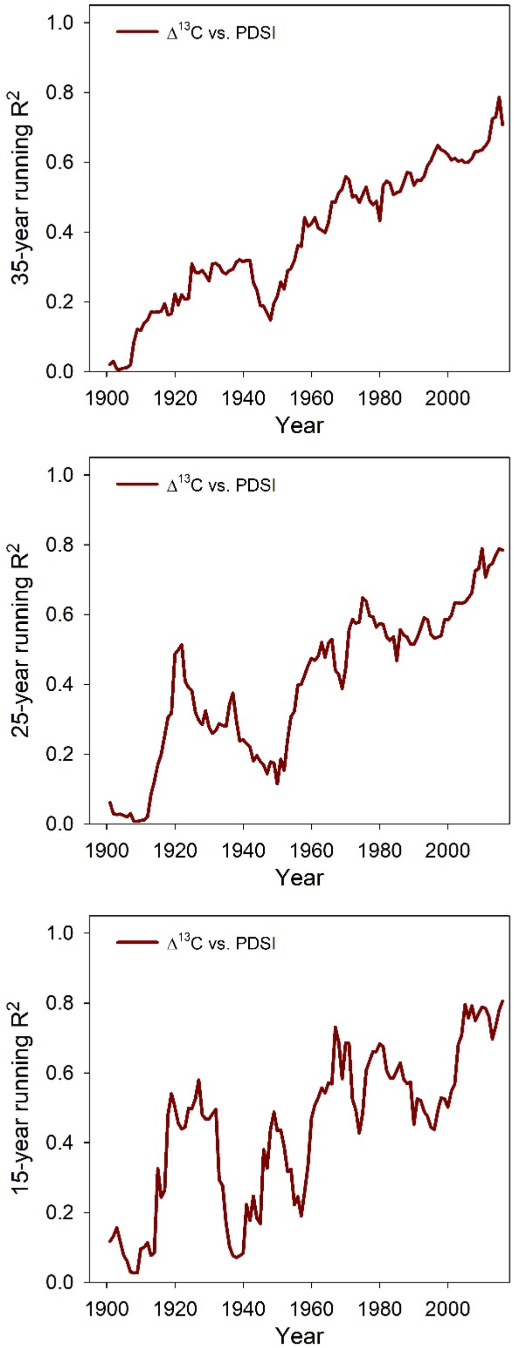

Supplementary Figure S2 – 35-year moving R^2 values from multiple regressions showing the amount of variation in pre-whitened $\Delta^{13}C$ explained by prewhitened VPD (A-B) and precipitation (C-D) for the current and previous year spanning the years 1900-2016. For each variable, colored lines combine two seasons centered on spring (spring/summer or spring/winter). Data near the ends of the moving window relationships shrink from 35 to 18 years in length

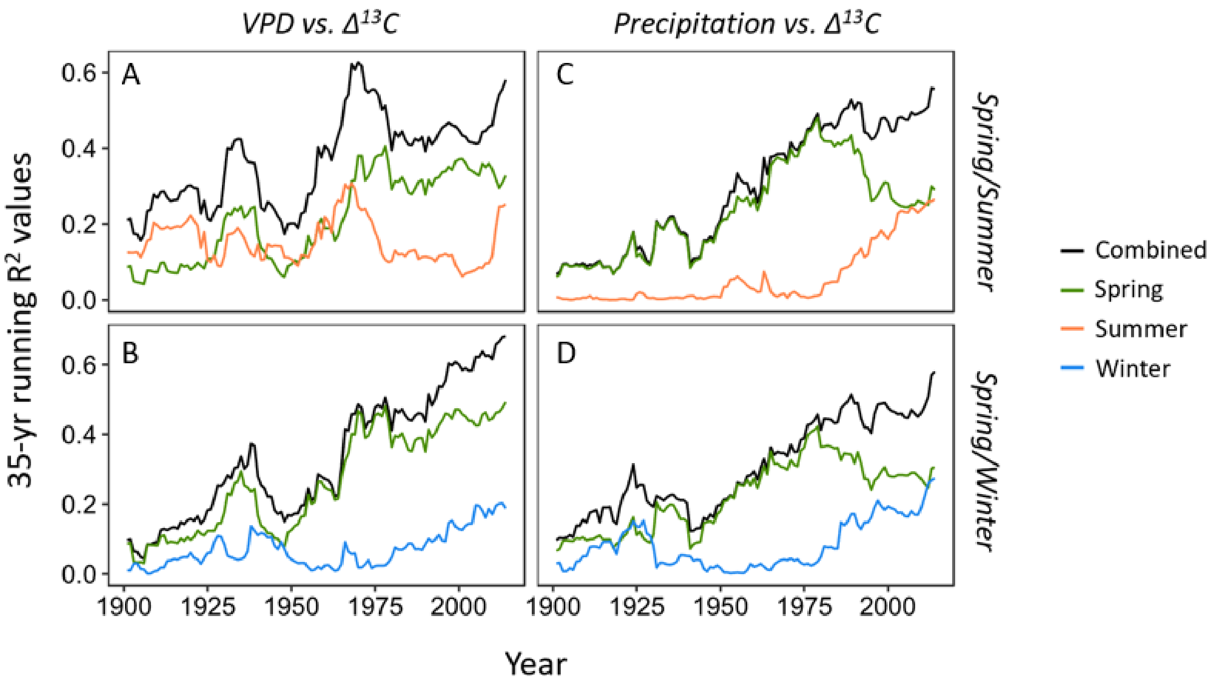

Supplementary Figure S3 – 35-year moving R^2 values from multiple regressions showing the amount of variation in pre-whitened ring-width index (RWI) values explained by VPD (A-B) and precipitation (C-D) for the years 1900-2016 for the current and previous year spanning the years 1900-2016. For each variable, colored lines combine two seasons centered on spring (spring/summer or spring/winter). Data near the ends of the moving window relationships shrink from 35 to 18 years in length.

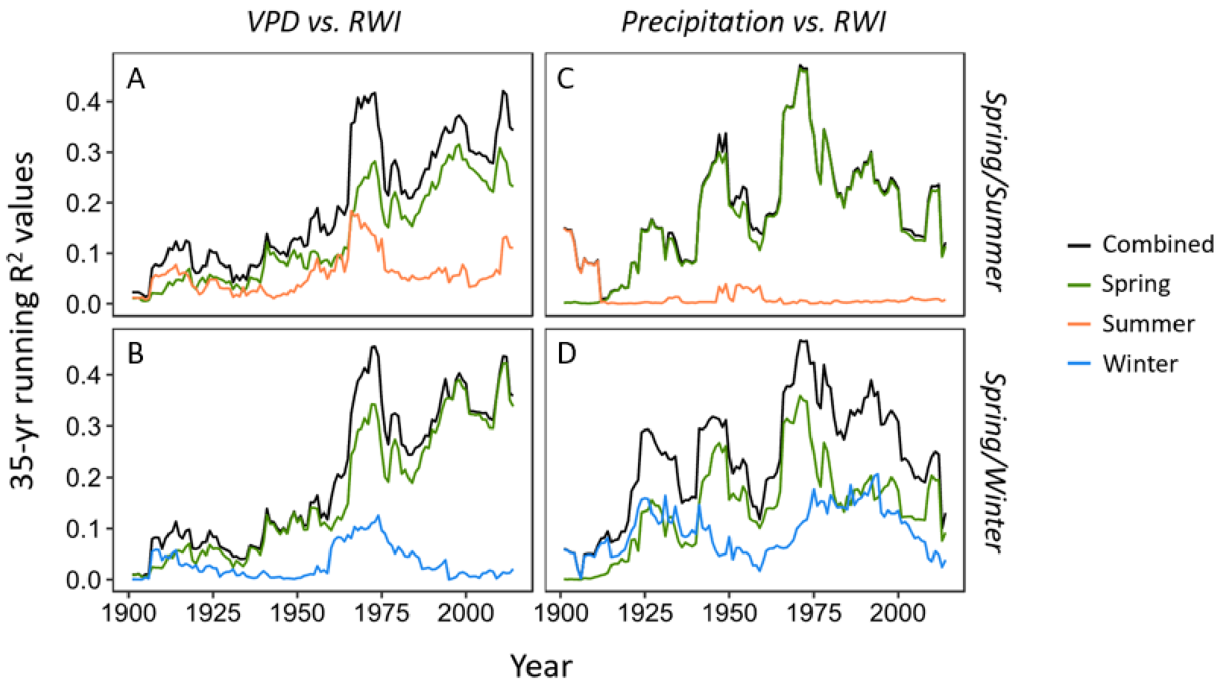

Supplementary Figure S4. – Percentage change in 35-year running variances of pre-whitened $\Delta^{13}C$ or ring-width index (RWI) where the baseline years were defined as 1901-1920). Data from sites with widespread mortality are plotted in shades of red and sites without substantial mortality are plotted in shades of blue.

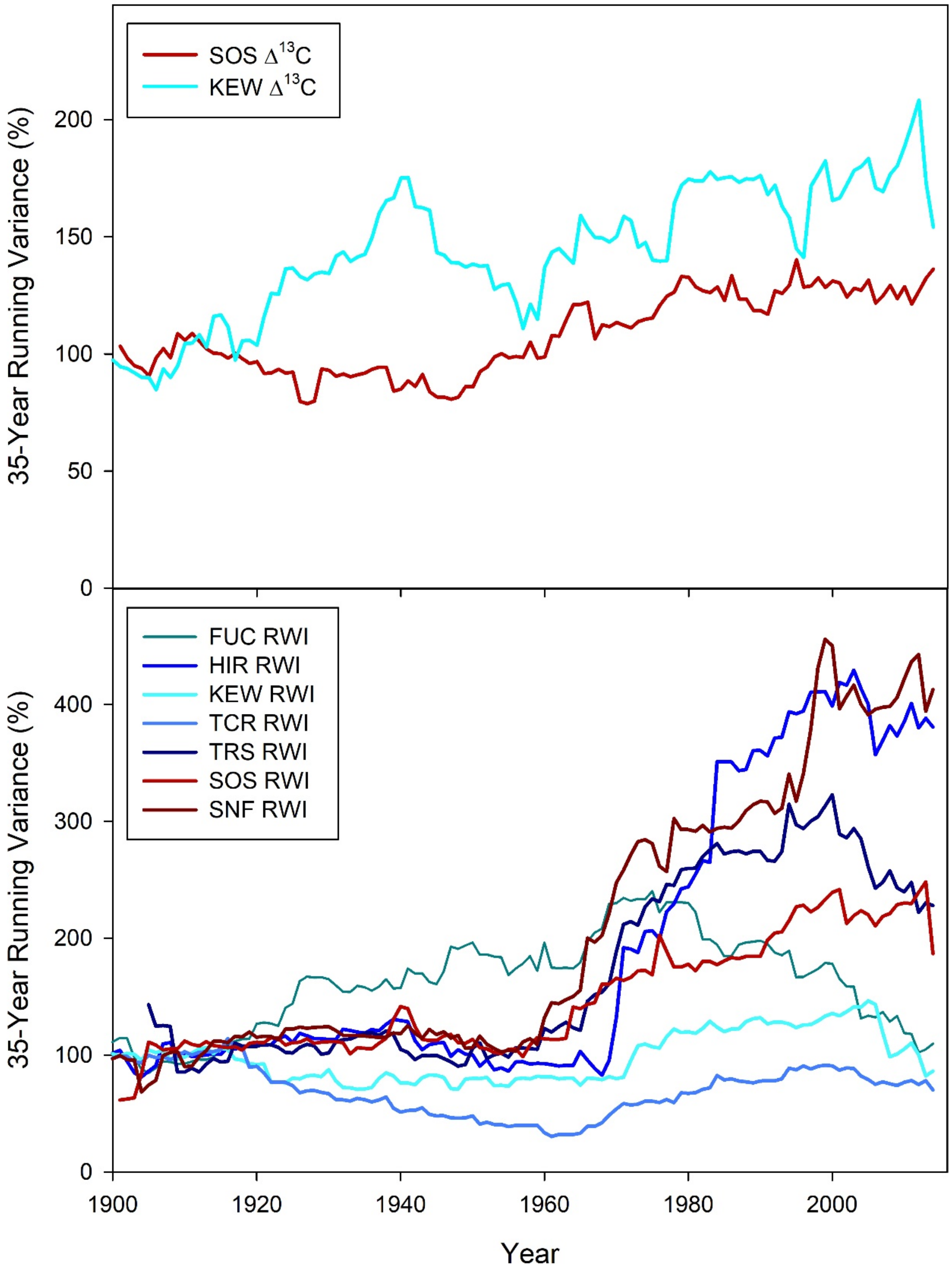

Supplementary Figure S5 – Summary of synthetic time series analyses demonstrating how quasi-linear increases of inter-annual variance of climate and tree-rings corresponds to non-linear increases in correlations and coefficients of determination. To conduct this analysis, we created 1000 pairs of synthetic time series spanning 250 years that included a mean pair-wise correlation of r = 0.40 over years 1 to 125. These time series included approximately 3.0-fold and 1.65-fold increases in variance of the synthetic inter-annual climate and tree-ring variables, respectively. The magnitude of variance amplification corresponds to that observed for PDSI for the southern Sierra Nevada region (i.e., approximately 3.0-fold) or ring-width index and latewood carbon isotope discrimination values (i.e., approximately 1.65-fold) over the period we present data for (i.e., 1901-2016). The correlated pairs of time series were synthesized with the following equations for each year; synthetic climate = $T \times R_1/A + R_1 \times B$, and synthetic tree-ring = $T \times R_1/A + R_2 \times B$. In these equations T is the timestep from 1 to 250, R_1 and R_2 were random numbers with values ranging from zero to one and A and B were constants set to control the magnitude of each variable and its associated variance.

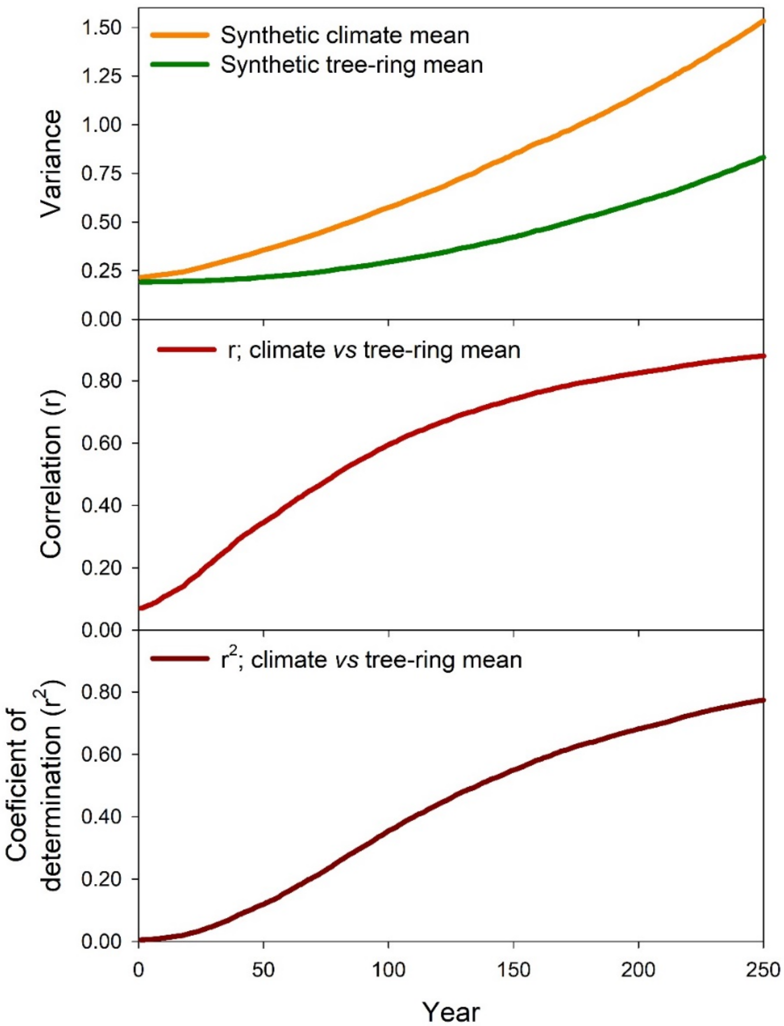

Supplementary Figure S6 – $\Delta^{13}C$ responses to summer (JJA) Palmer Drought Severity Index (PDSI) from this study (SOS) compared to that from two species at the KEW site in central Oregon. Data near ends of the moving window relationships shrink from 35 to 18 years in length.

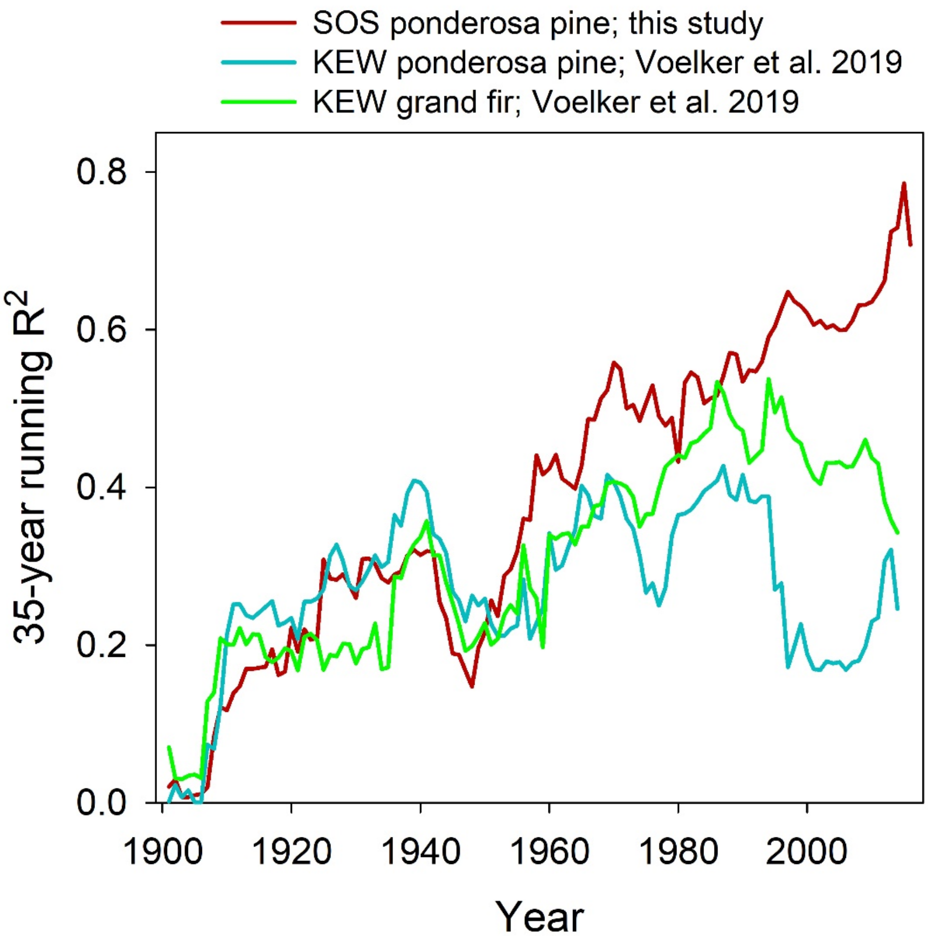

Figure S7. Spatial field correlation map of mean ring-width index and carbon isotope discrimination Z-scores (i.e., after Figure 3C) at the sampling location (blue cross) to inter-annual summer (June-August mean) leaf area index (LAI) values (left) and Moisture Control Factor (right) from 1984 to 2012, based on the data of Stöckli et al. (2011) model outputs. The 90% and 95% statistical confidence intervals are indicated at right of the correlation color scale. Model outputs were time-series of 1° gridded modeled LAI from summer (JJAS) climate reanalysis data spanning the years 1984 to 2012 (after Stökli et al. 2011; https://sourceforge.net/projects/phenoanalysis/). These gridded data were derived from was driven by daily gridded 1° climate data (temperature, radiation and VPD) and adjusted for 15 plant functional type classes. This prognostic model then employed ensemble data assimilation using Moderate Resolution Imaging Spectroradiometer (MODIS) satellite remote sensing data that were globally distributed to determine realistic parameterizations and reduce uncertainty for model predictions of LAI at sub-annual scales relevant for capturing broad scale seasonality across sites and inter-annual scales relevant for capturing the effects of drought and other factors on LAI.

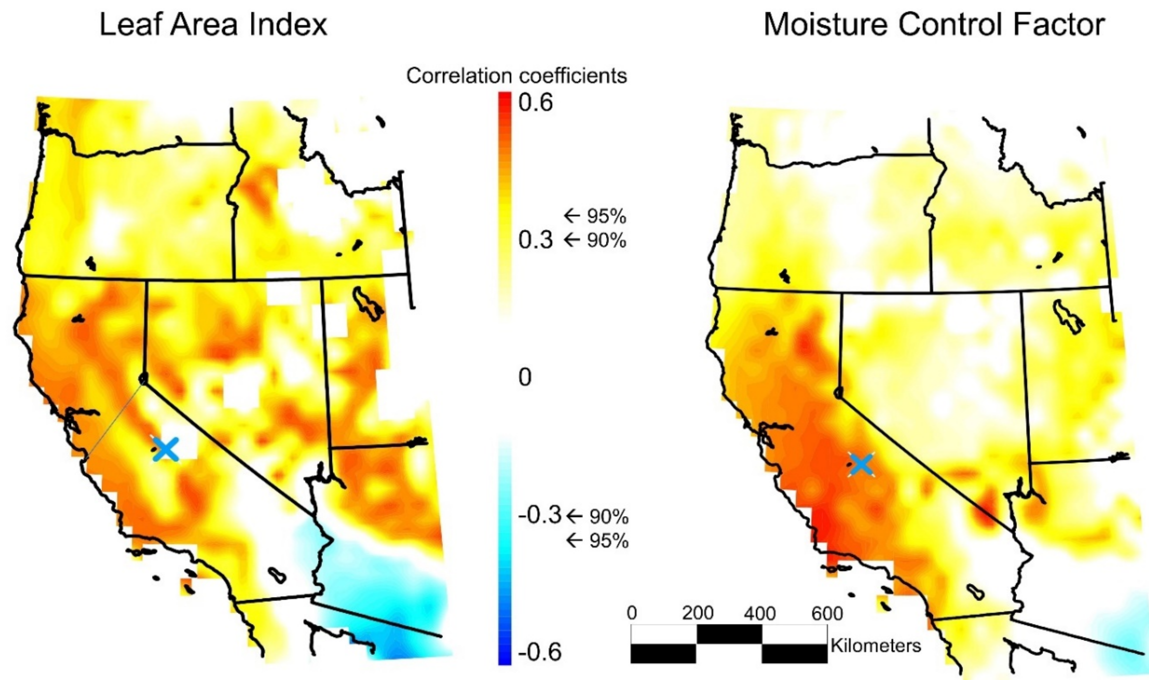

Literature Cited

Stöckli R., T. Rutishauser, I. Baker, M.A. Liniger and A.S. Denning. 2011. A global reanalysis of vegetation phenology. Journal of Geophysical Research Biogeosciences 116, G03020.